Variation of Cu Content of Sprayed Cu(In,Ga)(S,Se)$_2$ Solar Cells Based on a Thiol-Amine Solvent Mixture

Panagiota Arnou [1*], Soňa Uličná [1], Alexander Eeles [1], Mustafa Togay [1], Lewis D. Wright [1], Andrei V. Malkov [2], John M. Walls [1] and Jake W. Bowers [1]

[1] CREST, Wolfson School of Mechanical, Electrical and Manufacturing Engineering, [2] Department of Chemistry, Loughborough University, Leicestershire, LE11 3TU, UK

***Abstract*— Cu(In,Ga)(S,Se)$_2$ (CIGS) thin films were formed by a low cost solution-based approach using metal sulfide precursors. The stoichiometry of the absorber layer is tailored in order to improve film morphology and electrical properties. $Cu_yIn_{0.7}Ga_{0.3}Se_2$ films were prepared with a varied Cu content (0.8>y>1.1) and were completed in solar cell devices. The compositional, structural and electrical properties of the devices were investigated. Increased Cu content improves lateral crystallization, but results in the formation of Cu-rich secondary phases in-between CIGS grain boundaries. Characterization of the completed devices shows that Cu content has an important effect on the device electrical properties and the dominant recombination mechanisms.**

***Index Terms* —CIGS, low cost, solar cells, solution processing, stoichiometry**

I. Introduction

The chalcopyrite semiconductor $CuInSe_2$, along with its related alloys (CIGS), is a promising light absorbing material commonly used in thin film solar cells. Due to desirable material properties, such as high optical absorption, tunable bandgap and high stability, CIGS solar cells have the highest performance among thin film technologies [1]. CIGS solar modules are conventionally fabricated using well-established vacuum-based techniques, such as multi-stage co-evaporation or sputtering [1, 2]. Recently, there has also been increasing attention in atmospheric processes which are highly attractive for low cost production of photovoltaics.

The development of a hydrazine-based method was a breakthrough in the solution processing of CIGS [3]. High quality absorbers can be fabricated using this method, owing to the solvent properties of hydrazine and the excellent solubility of metal chalcogenides [3]. Nonetheless, the high toxicity and explosive nature of hydrazine raise safety concerns which hinder the potential for commercialization. A safer alternative solvent combination of a diamine and a dithiol has recently been found to effectively dissolve metal chalcogenides [4]. Following this work, molecular-based approaches have been developed for CIGS solar cells based on the amine-thiol system [5-8].

In previous work, we presented a straight-forward deposition technique for CIGS thin films, starting from metal sulfides dissolved in a mixture of 1,2-ethylenediamine (EDA) and 1,2-ethanedithiol (EDT) [5]. Addition of Ga metal in the starting solution allowed a fine bandgap adjustment and improved photovoltaic performance [6]. These devices were limited by the incomplete crystallization of the absorber and the formation of two separate layers after selenization, which is a common problem found in solution-based CIGS [5, 9].

The ratio of Cu to Ga+In (CGI) is known to have a strong effect on grain size in vacuum deposited films. Films with CGI>1 show much larger grains than films with CGI<1. This is thought to be due to the effect of Cu_xSe forming a quasi-liquid surface layer which acts as a fluxing agent [10]. Devices with CGI>1 however are usually dominated by interface recombination and have much lower efficiencies than devices with CGI<1 [11]. For this reason, most high performance devices undergo a Cu rich (CGI>1) stage during the film formation in order to promote grain growth, but are then eventually finished as Cu-poor with CGI in the range of 0.88 to 0.95 [2]. Alternatively, CIGS can be made as Cu-rich, followed by a chemical wet etching step to selectively remove Cu_xSe phases [11].

In this work we varied CGI in an effort to improve the crystal quality and fully recrystallize the absorber layer. The impact of the absorber composition on the film microstructure and solar cell properties is investigated.

II. Experimental

CIGS thin films were spray-deposited in ambient atmospheric conditions, using a similar approach to what has been reported previously [6]. Here, a constant GGI and a varied CGI were attempted. Different stock solutions were prepared for In_2S_3 (717mg In_2S_3, 10ml EDA, 1ml EDT), Cu_2S (350mg Cu_2S, 10ml EDA, 1ml EDT) and Ga precursor (107mg Ga, 243mg Se, 7ml EDA, 0.7ml EDT). In_2S_3 and Cu_2S precursor solutions were dissolved at room temperature, whilst the Ga precursor required mild heating at ~50°C. After dissolution, the three component solutions were mixed in predetermined ratios to form the CIGS precursor solution with the desired composition. The GGI ratio was fixed to 0.3 and the CGI ratio was varied from 0.8 to 1.1. The mixed precursor solution was left stirring for 3-4 hours. Before deposition, the precursor solution was diluted with ethyl acetate (2:1 v/v) and then filtered (0.45 μm PTFE).

The films were sprayed onto molybdenum-coated soda lime glass substrates placed on a hot plate, controlled at 310°C. A deposition/drying cycle was repeated 6 times. Unless otherwise stated, the same precursor solution was used for all the spray cycles. In one case, however, the first 3 sprayed layers were performed using the solution with CGI=1.0, followed by 3 layers with CGI=0.8. Layers of different stoichiometry were combined in order to promote elemental interdiffusion and improve recrystallization during the subsequent selenization step. A graded CGI profile can also result in a combination of the favourable interface properties of Cu-poor material and the improved crystal growth of Cu-rich material [11].

After the last deposition/drying cycle, a selenization step was performed inside a tube furnace, where two 2.5x2.5cm samples were placed inside a graphite box with Se pellets. The tube was first purged with nitrogen, after which the pressure was set to 450 Torr. The tube remained sealed during selenization in order to allow a higher Se partial pressure. A total heating time of 50min (~35°C/min) and a final temperature of 540°C resulted in a final pressure of ~770 Torr and evaporation of the entire Se amount (~300 mg).

Two sister samples of each composition were deposited and selenized in the same run. One sample of each pair was chemically etched for 30sec in a 10% KCN aqueous solution immediately before the CdS buffer layer deposition. Although the formation of Cu_xSe phases is unlikely for CGI<1, the KCN etch can have additional beneficial effects, such as recovery of the minority carrier lifetime for air-exposed samples [11]. The CdS layer (~60nm) was deposited by chemical bath deposition. The intrinsic ZnO and Al doped ZnO layers (~80nm and 500nm, respectively) were both deposited using RF sputtering. No contact grid or anti-reflective coatings were used in this configuration. Mechanical scribing was performed to define individual cells of ~0.25cm^2 area. Sodium is only unintentionally supplied from diffusion from the glass substrate.

Device J-V characterization was performed using an in-house solar simulator under 1000W/m^2 illumination. The film morphology was investigated using a Carl Zeiss 1530 VP field emission gun scanning electron microscope (FEGSEM) with 30 μm aperture size and 5 kV operating voltage. The grain size was measured offline from the SEM images using AxioVision software (release 4.9.1, Zeiss). Energy Dispersive X-ray spectroscopy (EDS) was used for compositional analysis, with an aperture size of 60 μm and 20 kV operating voltage. A Bruker D2 phaser X-ray diffractometer was used for X-ray diffraction (XRD) analysis, using a Cu-Kα X-ray source and a Lynxeye detector. Capacitance-voltage profiling (CV) was carried out using a Keysight E4990 Impedance Analyzer and four-point probes. The temperature was adjusted with a LakeShore 335 Temperature Controller through a Janis CCS-150 closed cycle helium cryostat. The current density-voltage (JVT) characteristics were measured at different temperatures using a Keysight B2902A unit under 500W/m^2 illumination.

III. Results

Five CIGS thin films were synthesized targeting a varied Cu content, as described in the experimental section. The targeted CGI varied from 0.8 to 1.1, with 0.1 increments. Additionally, one sample was prepared by combining solutions with CGI=1.0 and 0.8 (0.8/1.0).

The microstructure of the films was investigated. Fig. 1 shows the top view SEM images (left column), as well as the cross sectional images (right column) for each sample. For the Cu-rich sample (CGI=1.1), the SEM images after the KCN etch are also shown (1.1 E). The images of the etched samples for the rest of the compositions are omitted, as no influence is visible on the film microstructure.

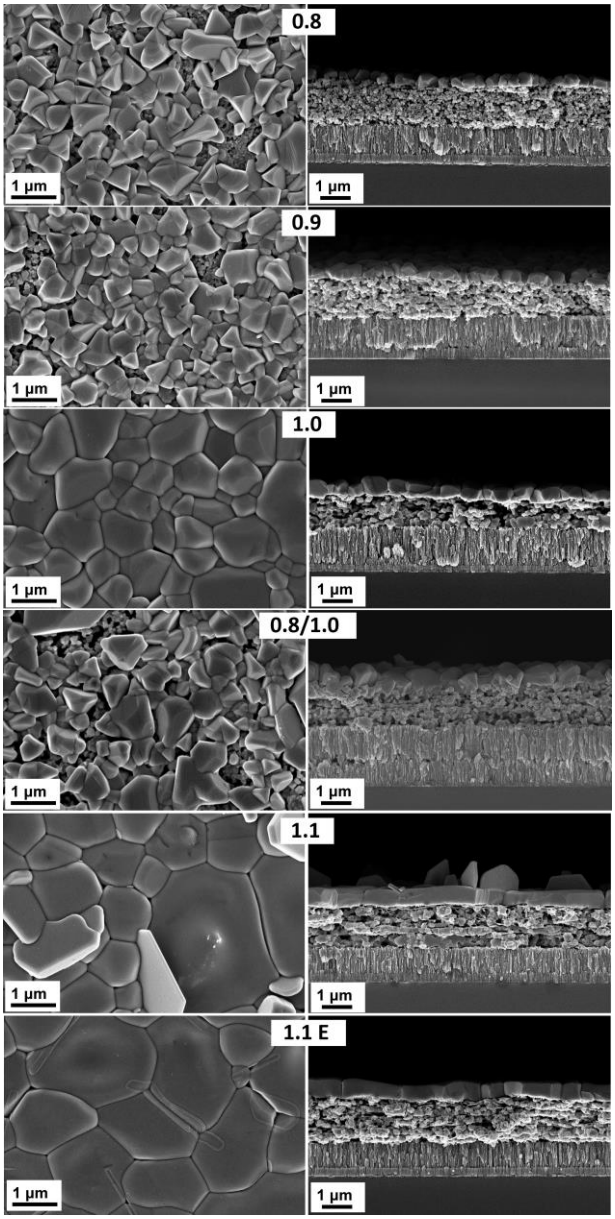

Fig. 1 Top-view (left) and cross section (right) SEM images of selenized CIGS layers with different CGI ratio.

The KCN etch dissolves the Cu_xSe secondary phases initially present on the Cu-rich sample. Surprisingly, this leaves behind a "chalk outline" on the film surface. It is still unclear whether this feature degrades device performance. Nonetheless, the KCN etch does not seem to form significant voids, which would be deleterious to the device performance.

In terms of the crystal quality, as anticipated, grain growth is significantly improved with CGI. The lateral grain size was increased from ~1.1 µm (CGI=0.8) to >3µm (CGI=1.1). The cross sectional images, however, show that the crystallized depth of the absorber remains fairly constant (500-700nm), despite the increased lateral grain size. Fig. 2 (top) shows the influence of the CGI ratio on the lateral and vertical grain size. The constant crystalline depth could suggest that the recrystallization is more likely limited due to non-optimum selenization or due to the presence of oxides/residual carbon in the film. Total carbon, hydrogen and nitrogen contents were determined for an as-deposited and a selenized sample with CGI=0.9, using a CE-440 CHN Elemental Analyzer (Exeter Analytical Inc., Europe). The as deposited sample contained a carbon, hydrogen and nitrogen content of 4.1, 0.7 and 2.1 at.% respectively, whilst the corresponding contents in the selenized sample were 1.1, 0.0 and 0.8 at.%. The low C content suggests that this is unlikely to cause the incomplete crystallization, as opposed to other atmospheric techniques with a C content of up to 60 at.% in the uncrystallised bottom layer [7]. Fig. 2 (bottom) shows the CGI and GGI ratios for each sample, as determined by EDS analysis. It is confirmed that the GGI ratio is fixed to ~0.3 and that the CGI ratio is increased.

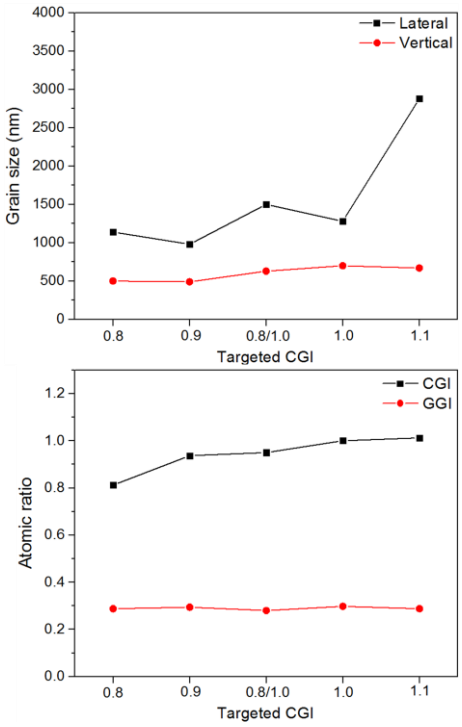

Fig. 2 Top: Lateral and vertical grain size for each sample. Bottom: CGI and GGI ratios for each sample, as determined by EDS.

The effect of the composition on the structural properties of CIGS films was characterized by XRD. Fig. 3 shows the XRD pattern of each sample. Each pattern consists of the same distinct peaks associated with the chalcopyrite structure of $CuIn_{0.5}Ga_{0.5}Se_2$ (JCPDS 40-1488), as well as peaks which correspond to Mo and $MoSe_2$. An additional peak is only evident at ~31.3° and it is removed after the KCN etch. This peak is likely associated with the Cu_xSe secondary phases. The inset table summarizes the position and the full width at half maximum (FWHM) of the (1 1 2) peak for each sample. The peak position remained unchanged, which suggest that the variation in the Cu content did not change the lattice parameters of the chalcopyrite structure. Finally, there is small decrease of the FWHM of the peak with CGI, which is consistent with the increase of the grain size, as shown by SEM imaging.

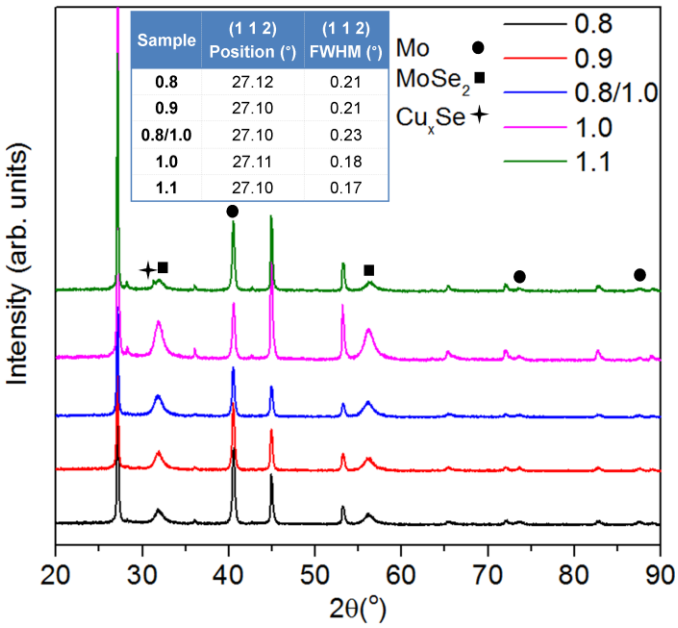

Fig. 3 XRD patterns of each selenized sample. Inset table: Summary of the (1 1 2) peak position and FWHM.

Fig. 4 shows the J-V curves of the highest performing cell of each sample. The J-V curves are considerably varied with Cu content. The Cu-poor samples have similar V_{oc} and J_{sc}, whilst these values are lower in the stoichiometric sample (CGI=1.0). This could be due to higher porosity in the bulk of the absorber, as seen in the cross sectional image of the stoichiometric sample, which could cause shunting losses. Additionally, the lower V_{oc} could be related to inferior interface properties. As expected, the Cu-rich sample exhibits a lower efficiency. This could be caused by shunting induced by the presence of a large amount of Cu_xSe secondary phases. However, the shunt resistance measured on the dark IV curve is not significantly high. This effect, as well as the fact that the KCN etch (designed to remove Cu_xSe) only marginally improves the performance, suggest that the performance loss is mostly caused by the inferior electronic properties of the Cu-

rich material. The best result was obtained for the graded sample (0.8/1.0 CGI) with an efficiency (η), fill factor (FF), open circuit voltage (V_{OC}) and short circuit current density (J_{SC}) of 9.0%, 50.2%, 547mV and 32.6mA/cm^2, respectively. This demonstrates the possibility of this technique to combine the larger grains from the stoichiometric layer with a Cu-poor overall composition. As previously discussed however there is another factor which limits the vertical grain growth. It should also be noted that FF is relatively low for all the samples due to series resistance losses caused by the thick $MoSe_2$ layer, the incompletely crystallized absorber, and the lack of a metallic collection grid. A barrier layer at the back contact is currently under development to control the $MoSe_2$ layer formation. This is expected to improve the FF of the devices and make the effect of the CGI clearer.

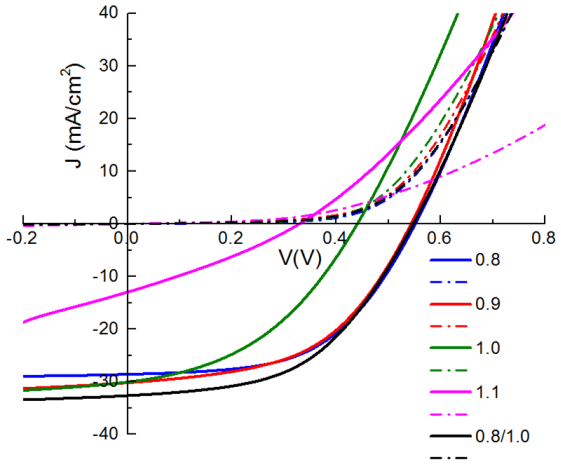

Fig. 4 J-V curves for the highest performing CIGS cells for each sample.

Statistical analysis was performed by measuring 6 adjacent cells on each sample. The J-V characteristics (η, FF, J_{SC}, V_{OC}) are summarized in the box plots of Fig. 5. It is evident that both η and FF values are decreased with CGI, as also seen in Fig. 4. J_{SC}, on the other hand, remains fairly constant, with the exception of the Cu-rich sample. The performance parameters of each sample after the 30sec etch are also included. Interestingly, the performance decreases for all the samples, apart from the Cu-rich, for which the improvement is marginal. This suggests that longer etching times could be required, which could also be associated with the presence of the outline features on the surface of the etched sample.

Fig. 6 shows the light and dark J-V curves at different temperatures for the sample with CGI=0.8. The light measurements were performed at a constant light intensity of 500W/m^2, using a halogen light source. The J-V curves for the rest of the samples are omitted as they have a similar behaviour. No roll-over of the J-V is observed at low temperatures indicating that there are no significant diode current barriers.

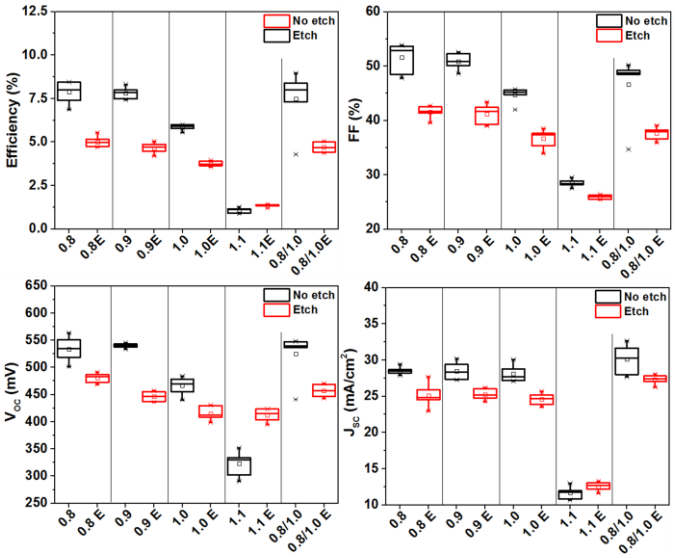

Fig. 5 Box plots summarizing the results from J-V measurements for each sample, before and after KCN etch.

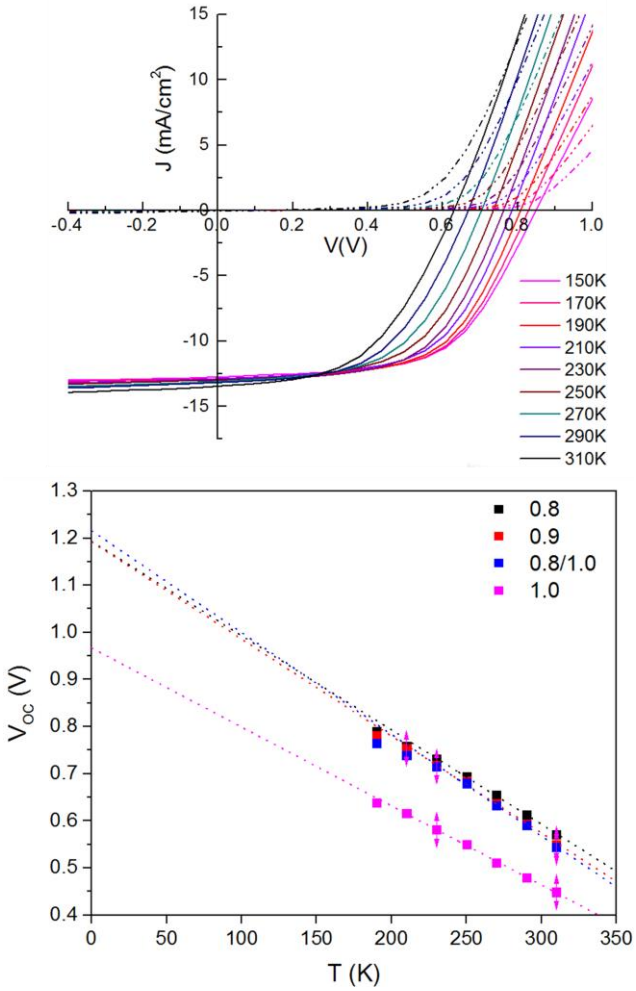

Fig. 6 Top: The light and dark J–V curves at varying temperatures from 150 to 310K for the sample with CGI=0.8. Bottom: Temperature dependence V_{OC} data for each sample, determined by the light J–V curves.

Fig. 6 shows the open circuit voltage as a function of temperature for each device. Extrapolation of Voc to 0K gives an activation energy for recombination E_a=qV of ~1..19 eV for CGI=0.8 and 0.9 and ~1..21 eV for CGI=0.8/1.0 [12]. These values are very similar to the expected bandgap of the material based on the empirical formula for $CuIn_{1-x}Ga_xSe_2$: E_g=1.65×+1.01(1-x)−0.151(1−x)x, with x=0.3 [13]. This indicates that the main recombination mechanism in these devices occurs in the bulk of the absorber, which is common for CIGS solar cells [3, 12]. In contrast, the extrapolation for the sample with CGI=1.0 gives a lower E_a of about ~0.97 eV. The fact that the E_a value is smaller than the bandgap of the absorber confirms that the device is limited by interface recombination rather than recombination in the bulk, which is the common result for stoichiometric devices [11]. The doping profile of each device was extracted from each CV curve at 300 K. These profiles (Fig. 7) indicate that the net doping density is higher in the stoichiometric film than in the Cu-poor, which is consistent with vacuum processed devices [11].

Based on these results, it is shown that the Cu content has a significant effect on the structural properties of the absorber film and the electrical properties of the solar cell device.

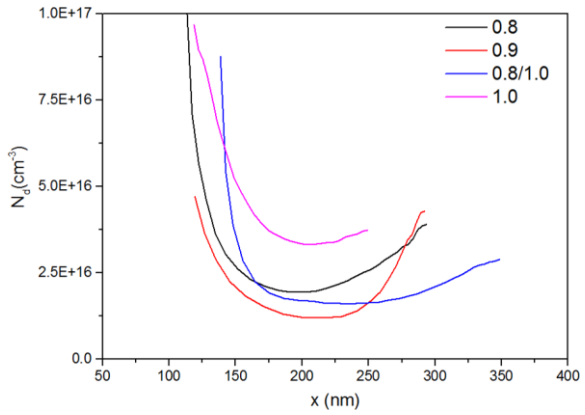

Fig. 7 Extracted doping profiles vs. distance from the junction for each CIGS sample, measured at 300 K.

III. Conclusions

The effects of CGI on the material and device properties of solution-processed CIGS were investigated. It was shown that good compositional control is possible using this deposition approach. The effect of CGI on the electrical properties of the devices was found to be similar to that seen in vacuum processes, with stoichiometric and Cu-rich devices dominated by interface recombination. Interestingly, the improved grain growth anticipated for higher CGI samples was observed only in the lateral direction, with the crystalline depth remaining fairly constant. Depositing a Cu-poor layer on top of a Cu-rich layer produced the highest efficiency by combining the larger crystals of the Cu-rich material with the favorable interface properties of a Cu-poor film. This device however was still limited by incomplete crystallization through the depth of the absorber.

Acknowledgement

The authors are grateful for funding from the EPSRC grant (EP/N026438/1) to support this work.

References

[1] R. Kamada, T. Yagioka, S. Adachi, A. Handa, K. F. Tai, T. Kato, and H. Sugimoto, “New world record Cu(In, Ga)(Se, S)2 thin film solar cell efficiency beyond 22%,” *2016 IEEE 43rd Photovoltaic Specialists Conference*, pp. 1287–1291, 2016.

[2] P. Jackson, D. Hariskos, R. Wuerz, O. Kiowski, A. Bauer, T. M. Friedlmeier, and M. Powalla, “Properties of Cu(In,Ga)Se2 solar cells with new record efficiencies up to 21.7%,” *Phys. Status Solidi RRL*, vol. 9, no. 1, pp. 28–31, Dec. 2014.

[3] T. K. Todorov, O. Gunawan, T. Gokmen, and D. B. Mitzi, “Solution-processed Cu(In,Ga)(S,Se)2 absorber yielding a 15.2% efficient solar cell,” *Prog. Photovolt Res. Appl.*, vol. 21, no. 1, pp. 82–87, 2012.

[4] D. H. Webber and R. L. Brutchey, “Alkahest for V2VI3 chalcogenides: dissolution of nine bulk semiconductors in a diamine-dithiol solvent mixture.,” *J. Am. Chem. Soc.*, vol. 135, no. 42, pp. 15722–15725, Oct. 2013.

[5] P. Arnou, M. F. A. M. Van Hest, C. S. Cooper, A. V. Malkov, J. M. Walls, and J. W. Bowers, “Hydrazine-Free Solution-Deposited CuIn(S,Se)2 Solar Cells by Spray Deposition of Metal Chalcogenides,” *ACS Appl. Mater. Interfaces*, vol. 8, no. 19, 2016.

[6] P. Arnou, C. S. Cooper, S. Uličná, A. Abbas, A. Eeles, L. D. Wright, A. V. Malkov, J. M. Walls, and J. W. Bowers, “Solution processing of CuIn(S,Se)2 and Cu(In,Ga)(S,Se)2 thin film solar cells using metal chalcogenide precursors,” *Thin Solid Films*, 2016.

[7] X. Zhao, M. Lu, M. Koeper, and R. Agrawal, “Solution-Processed Sulfur Depleted Cu(In,Ga)Se2 Solar Cells Synthesized from a Monoamine-Dithiol Solvent Mixture,” *J. Mater. Chem. A*, vol. 4, no. 19, pp. 7390–7397, 2016.

[8] D. Zhao, Q. Tian, Z. Zhou, G. Wang, Y. Meng, D. Kou, W. Zhou, D. Pan, and S. Wu, “Solution-deposited pure selenide CIGSe solar cells from elemental Cu, In, Ga, and Se,” *J. Mater. Chem. A Mater. energy Sustain.*, vol. 3, no. 38, pp. 19263–19267, 2015.

[9] I. Klugius, R. Miller, A. Quintilla, T. M. Friedlmeier, D. Blázquez-Sánchez, E. Ahlswede, and M. Powalla, “Growth mechanism of thermally processed Cu(In,Ga)S2 precursors for printed Cu(In,Ga)(S,Se)2 solar cells,” Phys. status solidi – Rapid Res. Lett., vol. 6, no. 7, pp. 297–299, 2012.

[10] R. Klenk, T. Walter, H.-W. Schock, and D. Cahen, “A model for the successful growth of polycrystalline films of CuInSe2 by multisource physical vacuum evaporation,” *Adv. Mater.*, vol. 5, no. 2, pp. 114–119, 1993.

[11] S. Siebentritt, L. Gütay, D. Regesch, Y. Aida, and V. Deprédurand, “Why do we make Cu(In,Ga)Se2 solar cells non-stoichiometric?,” *Sol. Energy Mater. Sol. Cells*, vol. 119, pp. 18–25, 2013.

[12] S. S. Hegedus and W. N. Shafarman, “Thin-film solar cells: device measurements and analysis,” *Prog. Photovoltaics Res. Appl.*, vol. 12, no. 2–3, pp. 155–176, 2004.

[13] B. J. Stanbery, “Copper Indium Selenides and Related Materials for Photovoltaic Devices,” *Crit. Rev. Solid State Mater. Sci.*, vol. 27, no. 2, pp. 73–117, Apr. 2002.